A measurement method of transverse light-shift in atomic spin co-magnetometer

Li Xing[1,2,*], Wei Quan[2,3], Tianxiao Song[4], Qingzhong Cai[2] and Wen Ye[5]

[1] *Division of Thermophysics and Process Measurements, National Institute of Metrology, NIM, Beijing 100029, China*
[2] *School of Instrumentation Science and Opto-electronics Engineering, Beihang University, Beijing 100191, China*
[3] *Beijing Academy of Quantum Information Sciences, Beijing 100191, China*
[4] *Beijing Institute of Space Launch Technology, China Academy of Launch Vehicle Technology, Beijing 100076, China*
[5] *Division of Mechanics and Acoustic Metrology, National Institute of Metrology, NIM, Beijing 100029, People's Republic of China*
*Corresponding author: xingli@nim.ac.cn

Abstract

We disclose a method to obtain the transverse light-shift along the probe light of a single-axis alkali metal-noble gas co-magnetometer. The relationship between transverse compensating field and light-shift is deduced through the steady-state solution of Bloch equations. The variety of probe light intensity is used to obtain the residual magnetic field, and step modulation tests are applied to acquire the total spin-relaxation rate of electron spins and self-compensation point. Finally, the transverse light-shift is reduced from -0.115 nT to -0.039 nT by optimizing the probe light wavelength, and the value of the calibration coefficient can be increased simultaneously.

1. Introduction

An alkali metal-noble gas co-magnetometer has found a wide range of applications in sensing rotation rate [1-3], testing Lorentz and CPT violation [4,5], and searching for anomalous spin-dependent forces [6,7]. In atomic spin co-magnetometers, the electron spins of alkali-metal are in SERF regime [8], so that the electron spins are ultra-high sensitive to magnetic field [9]. The nuclear spins of noble gas can be hyperpolarized by spin-exchange collisions with the polarized electron spins [10]. The polarized nuclear spins have ability of self-compensation to the external magnetic fields, and meanwhile the ultra-high sensitivity of rotation rate can be maintained [2]. However, the light-shift [11,12] arising from circularly polarized component of non-ideal linearly polarized probe beam can affect the direction and stability of electron spins [13,14]. Thus, the research on measurement and optimization of the transverse light-shift is essential for atomic spin co-magnetometers.

Recently, the influence of light-shift caused by the circularly polarized pump light of atomic spin co-magnetometer has been widely studied [15-17]. The light-shift interaction appears as a fictitious magnetic field, so that the atomic spins process around the total effective magnetic field [18]. Therefore, the light-shift should be minimized as far as possible. Moreover, the principle of light-shift caused by the pump light of a K-Rb-21Ne co-magnetometer has been analyzed [19], and the light-shift of Rb atoms can be reduced by collision mixing [11]. Furthermore, the light-shift would lead to cross-talk effect for a dual-axis co-magnetometer, which limits the measurement accuracy of the two sensitive axes [2,20]. However, there are few studies on transverse light-shift caused by the probe light of co-magnetometer, which has usually been ignored in the steady-state solution of Bloch equations [21,22]. With the improvement of the accuracy, the existence of the transverse light-shift cannot be neglected.

In this letter, we propose a method to measure the transverse light-shift based on the steady-state solution of Bloch equations through the variety of probe light intensity and transverse compensation magnetic field. The relationship between transverse light-shift and wavelength of the probe light has been studied, and we propose an optimization method for reducing the light-shift. Finally, the transverse light-shift has been reduced from -0.115 nT to -0.039 nT and the light-shift related term has been effectively suppressed. Meanwhile, the calibration coefficient of co-magnetometer has been concurrently increased.

2. Theory of the measurement method

The behavior of the K-Rb-^{21}Ne co-magnetometer can be represented by a set of Bloch equations. The evolutions of electron spin polarization $\mathbf{P}^e$ and nuclear spin polarization $\mathbf{P}^n$ can be described as below [1,2],

$$\frac{\partial \mathbf{P}^e}{\partial t} = \frac{\gamma_e}{Q(P^e)}\left(\mathbf{B}+\mathbf{B}_n+\mathbf{L}\right)\times\mathbf{P}^e - \mathbf{\Omega}\times\mathbf{P}^e + \frac{(R_p\mathbf{s}_p + R_{se}^{en}\mathbf{P}^n + R_m\mathbf{s}_m - R_{tot}^e\mathbf{P}^e)}{Q(P^e)}$$

$$\frac{\partial \mathbf{P}^n}{\partial t} = \gamma_n \left(\mathbf{B} + \mathbf{B}_e \right) \times \mathbf{P}^n - \mathbf{\Omega} \times \mathbf{P}^n + R_{se}^{ne} \left(\mathbf{P}^e - \mathbf{P}^n \right) - R_{sd}^n \mathbf{P}^n \tag{1}$$

where $\mathbf{\Omega}$ is the rotation velocity. $Q(P^e)$ is the slowing-down factor of electron. γ_e and γ_n are the gyromagnetic ratios of electron and nuclear spins, respectively. R_p and R_m are the pumping rates produced by the pump and probe lights. R_{se}^{ne} and R_{se}^{en} are the spin-exchange rates from electron to nucleus and from nucleus to electron, respectively. R_{tot}^e is the total spin-relaxation rate of electron spins, which is equal to $R_p + R_m + R_{se}^{en} + R_{sd}^e$. R_{sd}^e and R_{sd}^n are the electron and nuclear spin-destruction rate, respectively. $\mathbf{B}_e$ and $\mathbf{B}_n$ are the magnetic fields generated by the magnetizations of electron and nuclear spins. The electron spins process in the residual magnetic field $\mathbf{B}$. $\mathbf{L}$ is the light shift (AC-Stark shift) field, which is a magnetic-like field coupling to electrons generated by the detuned pump and probe lights. When the probe beam is along x-direction, the steady-state solution of Bloch equations about L_x can be simplified as follows,

$$P_x^e (L_x) \approx \frac{\gamma_e P_z^e R_{tot}^e}{R_{tot}^{e\,2} + \gamma_e^2 \left(L_z + \delta B_z \right)^2} [-\frac{\delta B_z}{B_n} \frac{L_x \gamma_e}{R_{tot}^e} B_c + \frac{\gamma_e L_x L_z}{R_{tot}^e} + o(10^{-6})] \tag{2}$$

where $\delta B_z = B_z - B_c$ is residual magnetic field along z-axis after the coil compensation. $B_c = -B_n - B_e$ is self-compensation point of the co-magnetometer to cancel the fields from nuclear and electron magnetization. The transverse light-shift L_x are mainly related to δB_z, and the longitudinal light shift L_z. It is approximated to a constant with the parameters of temperature and pump light invariant. Thus, the δB_z related terms of transverse electron spin polarization P_x^e in a K-Rb-^{21}Ne co-magnetometer can be deduced as,

$$P_x^e (\delta B_z) \approx \frac{\gamma_e P_z^e R_{tot}^e}{R_{tote}^2 + \gamma_e^2 \left(L_z + \delta B_z \right)^2} [-\frac{\delta B_z}{B_n} (B_y + \frac{L_x \gamma_e}{R_{tot}^e} B_c) + o(10^{-6})] \tag{3}$$

Once the compensation field of B_z has been found, the residual magnetic field B_y can be compensated by the coils. We note that B_y and L_x jointly determine whether the magnetic field along y-axis is zero. The value of transverse compensating magnetic field B_{yc} is equal to $-B_y - \frac{L_x \gamma_e}{R_{tot}^e} B_c$. Thus, when the residual magnetic field B_y is determined, the light shift L_x can be obtained. Considering total energy level splitting effect of the probe light on D1 and D2 lines of Rb atoms, the light shift L_x can be expressed by [11],

$$L_x = \frac{\Phi(v) r_e c}{A \gamma_e} \left(-f_{D1} \frac{\left(v_{probe} - v_{D1} \right)}{\left(v_{probe} - v_{D1} \right)^2 + \left(\Gamma_{D1} / 2 \right)^2} + f_{D2} \frac{\left(v_{probe} - v_{D2} \right)}{\left(v_{probe} - v_{D2} \right)^2 + \left(\Gamma_{D2} / 2 \right)^2} \right) s_x \tag{4}$$

where r_e is classical electron radius and c is light velocity. f_{D1} and f_{D2} are oscillator strength of D1 and D2 lines, respectively. s_x is ellipticity of the non-ideal probe light. $v_{D1,D2}$ are the D1

and D2 resonance lines, respectively. ν_{probe} is the frequency of probe beam. $\Gamma_{D1,D2}$ are broadening width under D1 and D2 resonance lines, respectively. $\Phi(\nu)/A$ is the luminous flux per unit area and per unit time, which is proportional to the light intensity. The $\left|L_x\right|$ increases linearly with the increasing of probe intensity, so that the relationship between transverse compensating field B_{yc} and probe intensity are linear. When the light intensity is zero, the light shift L_x can be zeroed at the same time and $B_{yc} = -B_y$. Therefore, the residual magnetic field B_y can be obtained by varying the intensity of probe light and deducing B_{yc} at the point of zero intensity light. Finally, the value of $L_x \gamma_e B_c / R_{tot}^e$ can be acquired by adding $-B_{yc}$ and $-B_y$. Moreover, the total relaxation rate R_{tot}^e and the compensation point B_c can be calculated by fitting the dispersion curves generated by B_y modulation as a function of δB_z. The step modulation output signals ΔS can be expressed as follows,

$$\frac{\Delta S}{\Delta B_y} = k \frac{P_e^z R_{tot}^e}{\gamma_e B_c} \cdot \frac{\delta B_z}{((\delta B_z + L_z)^2 + (R_{tot}^e / \gamma_e)^2)} \tag{5}$$

where k is a constant relating to the . Therefore, the transverse light-shift L_x can be calculated by,

$$L_x = -\frac{R_{tot}^e (B_{yc} + B_y)}{\gamma_e B_c} \tag{6}$$

According to Eq. (4), the relationship between probe light wavelength and transverse light shift L_x under different [21]Ne pressure can be simulated in Fig.1. Thus, the L_x can be reduced by optimizing the detuning of probe light wavelength.
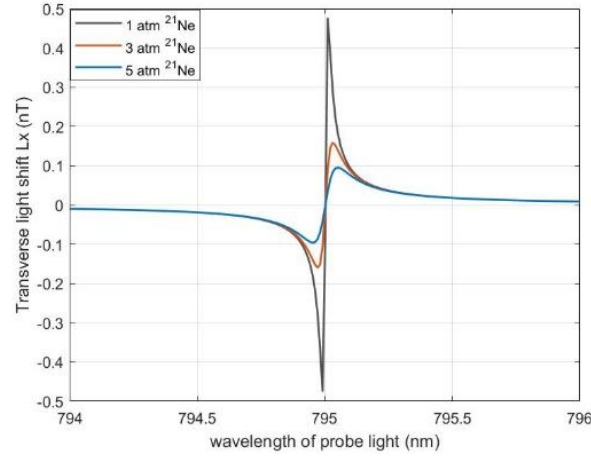
Fig.1. The simulation of the relationship between probe light wavelength and L_x under different pressure.
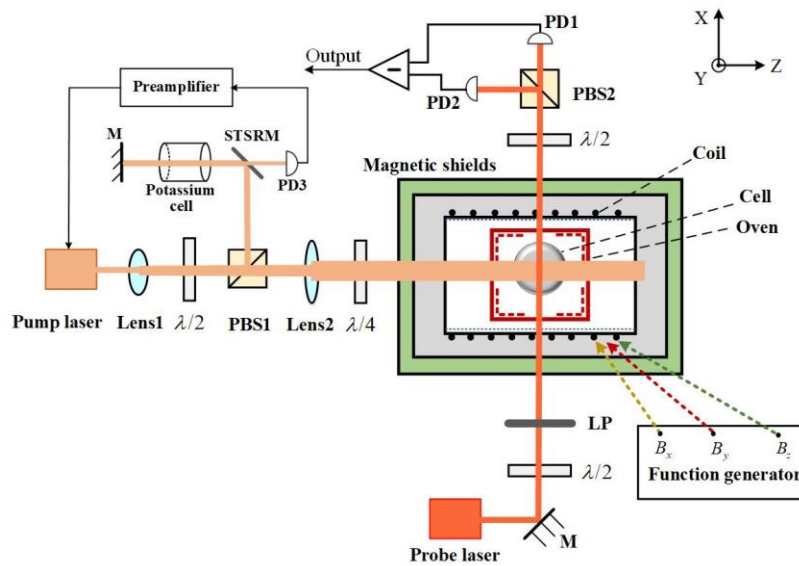
3. Experimental setup and results

Fig.2. Schematic diagram of the K-Rb-^{21}Ne co-magnetometer. Lens: plano-convex lens, LP: linear polarizer, M: reflection mirror, PBS: polarization beam splitter, STSRM: semi-transparent and semi-reflective mirror, PD: photodiode.

The schematic diagram of the K-Rb-^{21}Ne co-magnetometer is shown in Fig.2. The sensitive core is a 10-mm-diameter spherical cell, which contains a drop of K and Rb alkali metals, 3 atm of ^{21}Ne and 40 Torr of N_2 for quenching. The vapor cell is placed in an oven, which can heat the temperature of the cell to 180 °C. Three layers of μ^- metal magnetic shields surround the oven to provide a weak magnetic environment for atoms. A set of three-axis magnetic field coils is used to compensate residual fields in the shields.

A circularly polarized pump light along z-axis tuned on the K D1 resonance line is used to polarize the K atoms, and the Rb atoms are polarized through the spin-exchange collision among K atoms. The polarized alkali-metal atoms ultimately hyperpolarize the ^{21}Ne atoms [23]. A potassium vacuum cell is used to present the absorption spectrum, and the wavelength of pump light can be stabilized to the order of megahertz by

saturated absorption. Thus, the influence of pump light wavelength on light-shift can be ignored in our setup. A non-ideal linearly polarized probe beam detuned to the red side of Rb D2 line, which is orthogonal to the pump beam, is utilized to detect the variety of the transverse polarization of Rb atoms along x-axis. The probe beam contains elliptical polarization component due to the limitation of polarization performance of the polarizer, which can cause transverse light-shift along the probe beam. The relationship between probe light intensity and compensating field B_{yc} is shown in Fig.3. According to the linear fitting curves, the residual magnetic field B_y can be obtained by the intercept. The insert map shows measurement results of B_y under different light wavelength and the average value is 3.379 nT in this setup.
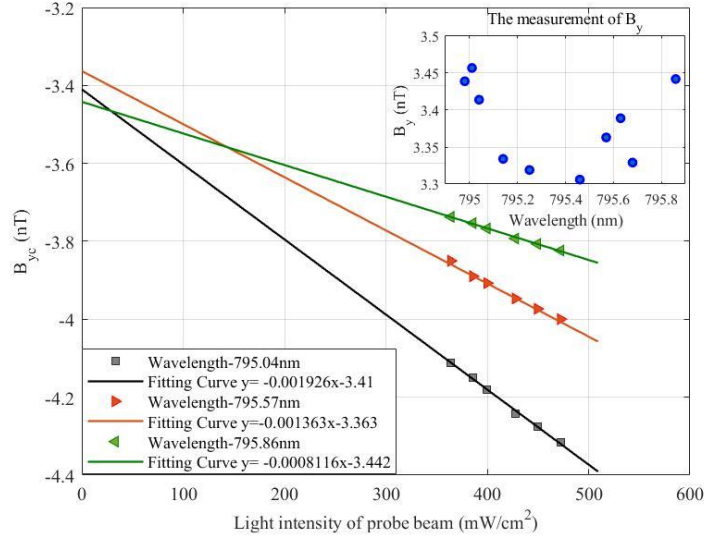

Fig.3. Relationship between the compensating field B_{yc} and the probe light intensity under different light wavelength. The residual magnetic field B_y can be obtained by the intercept.

The B_y step modulation output signals under different wavelength of the probe light have been tested in Fig.4. The R_{tot}^e / γ_e and B_c can be obtained by fitting the dispersion curves with Eq.(5), and the fitting results under different wavelength are shown in the insert map of Fig.4 and Fig.5, respectively. It is obvious that the values of R_{tot}^e / γ_e and B_c are influenced by the wavelength of probe light due to transverse pumping effect on the electron spins. According to the values of R_{tot}^e / γ_e and B_c, the light-shift L_x can be calculated by Eq.(6). The values of L_x and the related term $\frac{L_x \gamma_e}{R_{tot}^e} B_c$ under different wavelength of probe light are shown in Fig.5. The relationship between L_x and the wavelength of probe light is a Lorentz linear, and the effect of L_x can be magnified by the terms of R_{tot}^e / γ_e and B_c for about one order of magnitude. L_x has the most serious effect near the wavelength of 795 nm, which is at the transition frequency of Rb D2 line. When the wavelength is detuned to the red side of Rb D2 line, L_x decays exponentially and it is basically unchanged with the light wavelength larger than 795.6 nm. At 3 atm of ^{21}Ne, the

calibration coefficient of co-magnetometer firstly increases and then decreases with the increase of the light wavelength. The performance of the co-magnetometer can be optimized by reducing the influence of transverse light-shift L_x and meanwhile increasing the calibration coefficient. In our experiments, the L_x can be reduced from -0.115 nT to -0.039 nT by optimizing the wavelength of probe light to 795.68 nm. Meanwhile, the calibration coefficient is 26.19 V/°/s. When the wavelength is greater than 795.68 nm, the value of calibration coefficient gradually decreases and the value of L_x is almost invariant. Thus, the optimal wavelength of the probe light is 795.68 nm for our setup, and the related term $\dfrac{L_x \gamma_e}{R_{tot}^e} B_c$ can be reduced from 1.113 nT to 0.431 nT during the optimization routine.
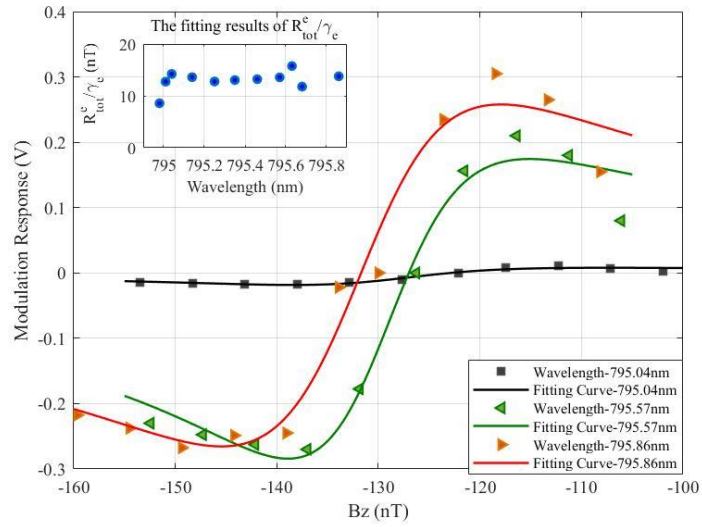

Fig.4. B_y step modulation output signals with different wavelength of the probe light. The fitting curves are derived from Eq.(5).
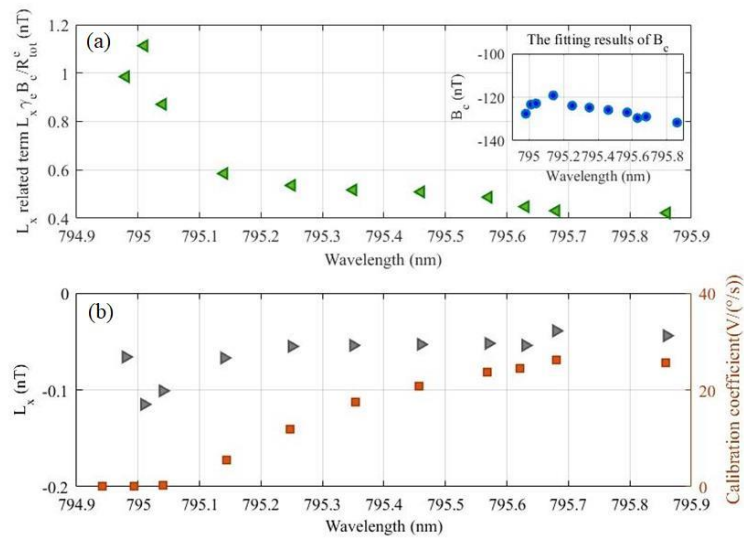

Fig.5. Optimization results of L_x, the related term $L_x \gamma_e B_c / R_{tot}^e$ and calibration coefficient. (a) The tests of related term $L_x \gamma_e B_c / R_{tot}^e$. The fitting results of B_c is derived from the data of Fig.5. (b) The test results of

L_x and calibration coefficient of the co-magnetometer.

4. Conclusion

In conclusion, a method for measuring the transverse light-shift has been examined in a compact K-Rb-^{21}Ne co-magnetometer. The value of the transverse light-shift L_x could be calculated by Eq.(6). The residual magnetic field B_y could be obtained by measuring the relationship between transverse compensating field B_{yc} and the intensity of probe light. In addition, other related parameters R_{tot}^e / γ_e and B_c could be obtained by fitting the B_y step modulation output signal ΔS. Finally, the transverse light-shift L_x has been reduced from -0.115 nT to -0.039 nT by optimizing wavelength of the probe light to 795.68 nm. Meanwhile, the related term $L_x \gamma_e B_c / R_{tot}^e$ has been reduced from 1.113 nT to 0.431 nT. Therefore, the influence of the transverse light-shift could be effectively restrained, which is beneficial to improve the accuracy of rotation rate measurement. Further improvement may be realized by properly increasing the pressure of ^{21}Ne in the vapor cell, which can directly inhibit the generation of transverse light-shift.

5. Acknowledgement

References

1. T. W. Kornack, R. K. Ghosh, and M. V. Romalis, Phys. Rev. Lett. 95, 230801 (2005).
2. R. Li, W. Fan, L. Jiang, L. Duan, W. Quan, and J. Fang, Phys. Rev. A 94, 032109 (2016).
3. M. Romalis and T. Kornack, (Princeton University Princeton United States, 2018).
4. F. Allmendinger, W. Heil, S. Karpuk, W. Kilian, A. Scharth, U. Schmidt, A. Schnabel, Y. Sobolev, and K. Tullney, Phys. Rev. Lett. 112, 110801 (2014).
5. M. Smiciklas and M. Romalis, (Meeting of the APS Division of Atomic American Physical Society, 2012).
6. L. Hunter, J. Gordon, S. Peck, D. Ang, and J.-F. Lin, Science 339, 928–932 (2013).
7. D. F. J. Kimball, J. Dudley, Y. Li, D. Patel, and J. Valdez, Phys. Rev. D 96, 075004 (2017).
8. J. C. Allred, R. N. Lyman, T. W. Kornack, and M. V. Romalis, Phys. Rev. Lett. 89, 130801 (2002).
9. W. Quan, W. Kai, and R. Li, Opt. Express 25, 130801 (2017).
10. R. K. Ghosh and M. V. Romalis, Phys. Rev. A 81, 043415 (2010).
11. Y. Chen, W. Quan, L. Duan, Y. Lu, L. Jiang, and J. Fang, Phys. Rev. A 94, 052705 (2016).
12. D. Miletic, C. Affolderbach, M. Hasegawa, R. Boudot, C. Gorecki, and G. Mileti, Appl. Phys. B 109, 89–97 (2012).
13. G. Vasilakis, Ph.D. thesis, Princeton University (2011).

14. I. A. Sulai, R. Wyllie, M. Kauer, G. S. Smetana, R. T. Wakai, and T. G. Walker, Opt. letters 38, 974–976 (2013).

15. K. Wei, T. Zhao, J. Fang, Y. Zhai, R. Li, and W. Quan, Opt. Express 27, 974–976 (2019).

16. C. Jia, C. Liu, D. Ming, C. Zhen, Y. Liang, and F. Wu, Appl. Phys. Lett. 116, 142405 (2020).

17. E. Zhivun, A. Wickenbrock, J. Sudyka, B. Patton, S. Pustelny, and D. Budker, Opt. Express 24, 15383–15390 (2016).

18. I. Novikova, A. B. Matsko, V. L. Velichansky, M. O. Scully, and G. R. Welch, Phys. Rev. A 63, 63802–63802 (2001).

19. J. Fang, S. Wan, Y. Chen, and R. Li, Appl. Opt. 51, 7714 (2012).

20. L. Jiang, W. Quan, R. Li, L. Duan, W. Fan, Z. Zhuo, F. Liu, L. Xing, and J. Fang, Phys. Rev. A 95, 062103 (2017).

21. R. Li, W. Quan, W. Fan, L. Xing, and J. Fang, Sensors Actuators A: Phys. 266, 130–134 (2017).

22. K. Wei, T. Zhao, J. Fang, R. Li, Y. Zhai, C. Han, and W. Quan, Phys. Rev. A 13, 044027 (2020).

23. R. K. Ghosh and M. V. Romalis, Phys. Rev. A 81, 043415–043415 (2010).